Available online at www.sciencedirect.com

ScienceDirect

Energy Procedia 48 (2014) 181 – 191

Energy Procedia

SHC 2013, International Conference on Solar Heating and Cooling for Buildings and Industry
September 23-25, 2013, Freiburg, Germany

Performance optimisation of polymeric collectors by means of dynamic simulation and sensitivity analysis

Christoph Reiter[a], Sebastian Brandmayr[a], Christoph Trinkl[a], Wilfried Zörner[a], Victor I. Hanby[b]

[a]*Technische Hochschule Ingolstadt, Institute of new Energy Systems (InES), Esplanade 10, Ingolstadt D-85049, Germany*
[b]*De Montfort University, The Gateway, Leicester LE1 9BH, United Kingdom*

Abstract

A dynamic flat-plate collector model for parametric sensitivity studies on polymer-based collector designs was developed. Validation using experimental results of conventional flat-plate collectors showed satisfying results especially regarding the calculation of individual part temperatures of a collector. The model was used to predict system efficiency as well as individual part temperatures in order to analyse a polymeric collector approach in comparison to a conventional collector. The simulation results showed that the fractional energy savings of systems with conventional flat-plate collectors cannot be reached with the analysed polymeric collector approach. Also the stagnation temperatures of more efficient approaches are too high for low-cost polymeric materials. The exemplary analysis of annual temperature loads of the backside insulation for different approaches proved the necessity of careful collector design aiming at temperature reduction for all individual collector parts.

Selection and peer review by the scientific conference committee of SHC 2013 under responsibility of PSE AG

Keywords: Mathematical Model; Simulation; Flat-Plate Collector; Collector Efficiency; Stagnation Temperature, Polymeric Materials

1. Background and proceeding

Manufacturers of solar-thermal systems aim at cost reduction especially regarding the collector. Significantly, increased market prices for aluminium and copper continuously obstruct these efforts. Against this background, the use of low-cost polymers in solar-thermal collectors offers cost and technical advantages. Besides that, polymeric collectors show remarkable properties in terms of handling and roof installation because of lightweight construction and freedom of design. Today's polymer manufacturing opportunities enable extensive production automation and hold considerable cost reduction potential. Nevertheless, high thermal loads on the collector parts are likely to be the

1876-6102
Selection and peer review by the scientific conference committee of SHC 2013 under responsibility of PSE AG
doi:10.1016/j.egypro.2014.02.023

main hurdle for the use of commodity plastics. Hence, in-depth analyses of short-term maximum as well as annual thermal loads on the individual parts of a collector, i.e. absorber, glazing, frame and backside, are required.

Based on the development of a dynamic collector model, a simulation study was carried out aiming at the investigation of a polymeric collector approach with regard to thermal loads and fractional energy savings. The simulations were performed using the simulation environment Matlab/Simulink [1] in combination with the CARNOT toolbox [2].

2. Collector modeling

Commonly used parameter models based on collector test results are not suitable for the investigation of collector design parameters. Also the steady-state Hottel-Whillier-Bliss model [3] only provides information about the collector performance by the fluid temperature. The part temperatures and the derived heat transfer coefficients have to be calculated by iterations. Thus, a dynamic model considering the relevant capacities was developed in order to derive information on individual part temperatures, heat fluxes and collector performance. Moreover, the model can be adjusted to new collector parameters or designs.

The five-node collector model considers the capacity of absorber (front and back plate), fluid, glazing and casing. The energy network connecting the nodes as well as the ambience are physical functions depending on geometry, size, materials and operating conditions. The cross section of the collector model is shown in Figure 1. The model basically represents a collector with a fully volumetric absorber but was for validation changed to a collector with sheet-pipe absorber. In the following the energy fluxes of the model are described in detail.

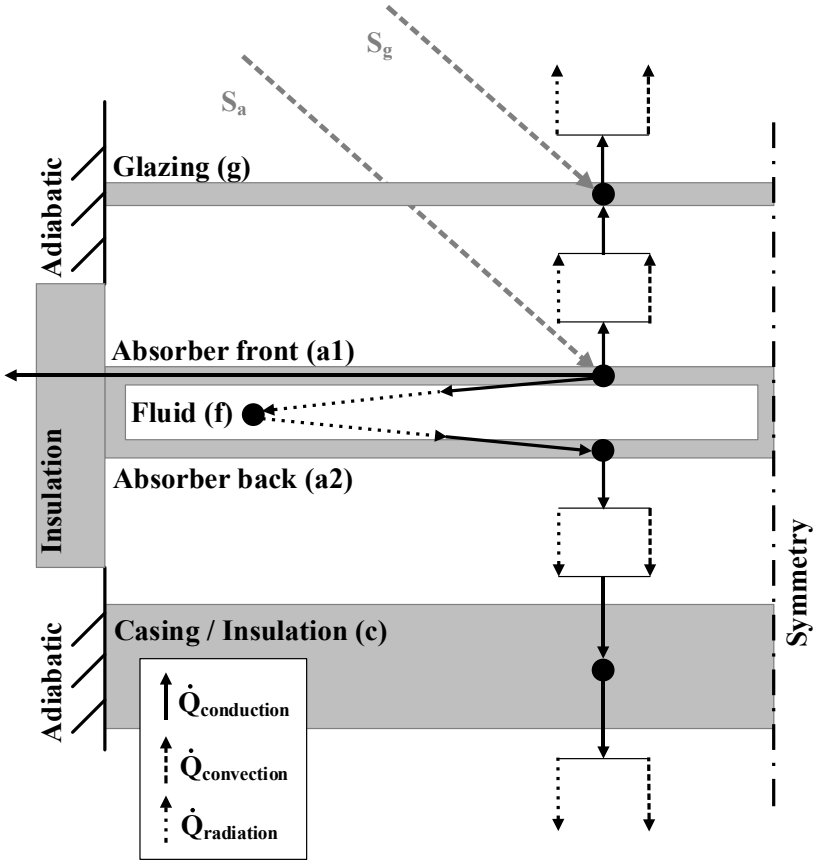

Fig. 1. Cross section of the collector model with nodes and energy fluxes

Nomenclature

Symbols:

A	area	[m^2]
Nu	Nusselt number	[-]
G	solar irradiance	[Wm^{-2}]
L	characteristic length	[m]
Pr	Prandtl number	[-]
$\dot{Q}$	heat flow rate	[W]
R_{th}	thermal resistance	[m^2KW^{-1}]
Ra	Rayleigh number	[-]
Ra_{crit}	critical Rayleigh number	[-]
Re	Reynolds number	[-]
S	absorbed solar radiation	[W]
dT	temperature change	[K]
T	temperature	[K]
c	specific heat capacity	[$kJkg^{-1}K^{-1}$]
dt	per time unit	[s]
f_{Pr}	Prandtl number correction factor	[-]
f_β	collector slope correction factor	[-]
f_{sav}	fractional energy savings	[%]
h	heat transfer coefficient	[$Wm^{-2}K^{-1}$]
k	heat conductivity	[Wm^{-1}]
m	mass	[kg]
$\dot{m}$	mass flow	[kgs^{-1}]
re	reflection coefficient	[-]
s	thickness	[m]
u	velocity	[ms^{-1}]
α	absorption coefficient	[-]
β	collector slope	[°]
γ	intermittency factor	[-]
ε	emission coefficient	[-]
ζ	friction factor	[-]
ν	kinematic viscosity	[m^2s^{-1}]
σ	Stefan-Boltzmann constant	[-]
τ	transmission coefficient	[-]

Subscripts:

a1	absorber front
a2	absorber back
air	air
amb	ambient
c	casing
cond	heat conduction
conv	convection
diff	diffuse
edge	collector edge
f	fluid
forced	forced
free	free
g	glazing
in	inlet / previous node
lam	laminar flow
rad	radiation
stag	stagnation
sky	sky / atmosphere
turb	turbulent flow
wind	wind

2.1. Energy balance

The equations (1) to (5) give an overview on the energy balance drawn in the collector model. The equations describe the capacities of each node as well as the energy fluxes of the nodes.

Glazing (g): $$m_g * c_g * \frac{dT_g}{dt} = S_g + \dot{Q}_{a1-g} - \dot{Q}_{g-amb} \quad (1)$$

Absorber front (a1): $$m_{a1} * c_{a1} * \frac{dT_{a1}}{dt} = S_{a1} - \dot{Q}_{a1-f} - \dot{Q}_{a1-g} - \dot{Q}_{a1-edge} \quad (2)$$

Fluid (f): $$m_f * c_f * \frac{dT_f}{dt} = \dot{m}_f * c_f * \left(T_{in} - T_f\right) + \dot{Q}_{a1-f} - \dot{Q}_{f-a2} \quad (3)$$

Absorber back (a2): $$m_{a2} * c_{a2} * \frac{dT_{a2}}{dt} = \dot{Q}_{f-a2} - \dot{Q}_{a2-c} \quad (4)$$

Casing / Insulation (c): $$m_c * c_c * \frac{dT_c}{dt} = \dot{Q}_{a2-c} - \dot{Q}_{c-amb} \quad (5)$$

2.2. Optical properties

The optical properties of the collector comprise the behavior of the absorber as well as the glazing under irradiance. Equation (6) describes the energy input at the absorber reduced by the effective transmission absorption product $(\tau\alpha)_{eff}$ of glazing and absorber [4].

$$S_{a1} = (\tau\alpha)_{eff} * A * G \quad (6)$$

Simple approaches of $(\tau\alpha)$ consider only the light transmission through the glazing and the absorption of the absorber surface. In this model the effective transmission absorption product $(\tau\alpha)_{eff}$, a more detailed approach is applied (cf. equation (7)). The multiple reflections between absorber and glazing are considered with non-ideal absorption coefficient α of the absorber and the diffuse reflection coefficient of the glazing re_{diff} [4].

$$(\tau\alpha)_{eff} = \frac{\tau * \alpha}{\left(1 - (1 - \alpha) * re_{diff}\right)} \quad (7)$$

The additional solar energy input in the glazing depending on absorption of the glazing changes the temperature of this node and influences the collectors' heat losses [3] (cf. equation (8)).

$$S_g = (1 - \tau_a) * A * G \quad (8)$$

2.3. Convection

Heat transfer by convection occurs at several layers in the collector. There is forced convection in the absorber caused by the heat transfer fluid and at the surface of the glazing caused by wind. Free convection occurs in the air gaps in front of the absorber and behind the absorber as well as at the glazing and at the backside of the collector. These heat transfer mechanisms are represented by equation (9) containing the convective heat transfer coefficient from equation (10), depending on the Nusselt number Nu and the characteristic length L of the part as well as on the heat conductivity k of the fluid [5].

$$\dot{Q}_{conv} = h_{conv} * A * (T_1 - T_2) \quad (9)$$

$$h_{conv} = \frac{Nu * k}{L} \quad (10)$$

The forced convection in the absorber channels was calculated according to the approach recommended by Mills [6] for forced convection in parallel plate ducts. Therefore, the characteristic length L is the doubled gap height instead of the commonly used pipe diameter and the transition from laminar flow starts at a Reynolds number of 2,800 instead of 2,300.

Hydrodynamically developed laminar flow for Reynolds numbers below 2,800 is set to the constant Nusselt number 5.385 [6]. In the transition region between laminar and fully developed turbulent flow with Reynolds numbers of 2,800 and 10,000 the Nusselt number is calculated by the equations (11) to (16) [7].

$$Nu_f = (1-\gamma) * Nu_{lam,2800} + \gamma * Nu_{turb,10^4} \tag{11}$$

$$\gamma = \frac{\mathrm{Re} - 2800}{10^4 - 2800} \quad and \quad 0 \le \gamma \le 1 \tag{12}$$

$$Nu_{lam,2800} = \sqrt[3]{49.371 + (Nu_{lam,2,2800} - 0.7)^3 + Nu^3_{lam,3,2800}} \tag{13}$$

$$Nu_{lam,2,2800} = \sqrt[3]{1.615 * \left(2300 * \mathrm{Pr} * \frac{d}{l}\right)} \tag{14}$$

$$Nu_{lam,3,2800} = \sqrt[6]{\frac{2}{1+22*\mathrm{Pr}}} * \sqrt{2300 * \mathrm{Pr} * \frac{d}{l}} \tag{15}$$

$$Nu_{turb,10^4} = \frac{\frac{0.0308}{8} * 10^4 * \mathrm{Pr}}{1 + 12.7 * \sqrt{\frac{0.0308}{8}} * \left(\mathrm{Pr}^{\frac{2}{3}} - 1\right)} * \left(1 + \left(\frac{d}{l}\right)^{\frac{2}{3}}\right) \tag{16}$$

The Nusselt number for fully developed turbulent flow is described by equation (17) and (18) [8].

$$Nu_f = \frac{\frac{\xi}{8} * \mathrm{Re} * \mathrm{Pr}}{1 + 12.7 * \sqrt{\frac{\xi}{8}} * \left(\mathrm{Pr}^{\frac{2}{3}} - 1\right)} * \left(1 + \left(\frac{d}{l}\right)^{\frac{2}{3}}\right) \tag{17}$$

$$\xi = (1.8 * \log_{10} \mathrm{Re} - 1.5)^{-2} \tag{18}$$

The convection on the outer surface of the glazing is a combination of free and forced convection shown in equation (19) [5].

$$Nu_{g-amb} = \sqrt[3]{Nu^3_{free,g-amb} + Nu^3_{forced,g-amb}} \tag{19}$$

The Nusselt number of the forced convection is considered according to equation (20) [9]. The average Reynolds number in equation (21) is calculated by the wind velocity u_{wind}, the characteristic length of the glazing $L_{g\text{-}amb}$ and the kinematic viscosity v_{air}.

$$Nu_{forced,g-amb} = \frac{0.037 * \mathrm{Re}^{0.8} * \mathrm{Pr}}{1 + 2.443 * \mathrm{Re}^{-0.1} * \left(\mathrm{Pr}^{\frac{2}{3}} - 1\right)} \tag{20}$$

$$\mathrm{Re} = \frac{u_{wind} * L_{g-amb}}{v_{air}} \tag{21}$$

Free laminar convection at the glazing with heat transfer upwards is defined in equation (22) by using a correction factor f_{Pr} from equation (23) for Prandtl numbers [10]. The laminar flow occurs for Rayleigh numbers below the critical Rayleigh number depending from the collector slope β from equation (24). The characteristic length $L_{c\text{-}amb}$ is in this case the length of the glazing.

$$Nu_{free,g-amb} = \left(0.825 + 0.387 * \sqrt[6]{Ra * \sin\beta * f_{\mathrm{Pr}}}\right)^2 \quad for \quad Ra < Ra_{crit} \tag{22}$$

$$f_{\mathrm{Pr}} = \left(1 + \left(\frac{0.492}{\mathrm{Pr}}\right)^{\frac{9}{16}}\right)^{-\frac{16}{9}} \quad for \quad 0.001 < \mathrm{Pr} < \infty \tag{23}$$

$$Ra_{crit} = 10^{\left(8.9 - 0.00178 * (90^\circ - \beta)^{1.82}\right)} \tag{24}$$

Free turbulent convection at the glazing with heat transfer upwards is calculated by equation (25) [10].

$$Nu_{turb,g-amb} = 0.56 * \left(Ra_{crit} * \cos(90° - \beta)\right)^{0.25} + 0.13 * \left(\sqrt[3]{Ra} - \sqrt[3]{Ra_{crit}}\right) \quad (25)$$

Duffie and Beckmann [2] assumed the heat transfer from the casing to the ambience by radiation and convection as negligible because of the major influence of the backside insulation and the resulting low temperature. In this model the heat transfer coefficients from the backside to the surroundings are calculated for an assumed windless region between collector and roof by radiation and natural convection. The Nusselt number for free convection with heat transfer downwards at the outer surface of the casing is described by the equations (22) and (23) [5]. The characteristic length $L_{c\text{-}amb}$ is in this case the length of the casing.

Free convection between glazing and absorber is shown in equation (26). Matuska and Zmrhal [11] derived a Nusselt correlation from several correlations like from Hollands [12] to verify the Nusselt number approach for a bigger range of collector slopes β (0° to 90°). The value of f_β in equation (27) is an angle factor for the Nusselt number depending on the collector slope which was obtained as quadratic function in the derived correlation.

$$Nu_{a1-g} = f_\beta * Ra^{0.29} \quad (26)$$

$$f_\beta = 0.1464 - 2.602 * 10^{-4} * \beta - 2.046 * 10^{-6} * \beta^2 \quad (27)$$

The Nusselt number for free convection between absorber and casing an approach from Arnold et al. [13] was applied for heat transfer downwards in enclosed air layers. Therefore, equation (28) is used for a heat transfer downwards. The basis is the calculated Nusselt number for heat transfer in vertical air layers (β=90°) between absorber backside and casing derived from equation (26) and (27).

$$Nu_{a2-c} = 1 + \left[Nu_{a2-c}(\beta = 90°) - 1\right] * \sin(180° - \beta) \quad (28)$$

2.4. Radiation

The heat transfer by radiation of two parallel plates is given from the Stefan-Boltzmann law in equation (29). This radiation exchange is necessary for the set-up of glazing and absorber front, absorber back and casing as well as casing and roof. The heat transfer coefficient for radiation is described in equation (30).

$$\dot{Q}_{rad} = h_{rad} * A * (T_1 - T_2) \quad (29)$$

$$h_{rad} = \frac{\sigma}{\left(\frac{1}{\varepsilon_1} + \frac{1}{\varepsilon_2} - 1\right)} * \left(T_1^2 + T_2^2\right) * (T_1 + T_2) \quad (30)$$

The radiation between glazing and cold sky is shown in equation (31). The emitted heat from the sky is neglected because of the infinite area of the sky's half-space [4].

$$h_{rad,g-sky} = \sigma * \varepsilon_g * \left(T_g^2 + T_{amb}^2\right) * \left(T_g + T_{amb}\right) \quad (31)$$

2.5. Heat conduction

Heat conduction occurs at glazing, absorber and casing. In the model the heat conduction connects the heat transfer from convection and radiation to the solid materials. Equation (32) and (33) describe the heat transfer depending from the heat conductivity k and the thickness s of the part [5]. Thin plates in the thermal network like glazing or absorber can be neglected because of the little influence on the overall heat transfer coefficients.

$$\dot{Q}_{cond} = h_{cond} * A * (T_1 - T_2) \quad (32)$$

$$h_{cond} = \frac{k}{s} \quad (33)$$

2.6. Edge losses

The edge losses cannot be mathematically calculated in detail. Duffie and Beckman [3] describe an approach considering the losses proportionally to the ratio between collector surface and edge surface. These losses are only connected to the absorber node converting irradiance. The other nodes have an adiabatic behavior against the edge neglecting the heat transfer coefficients from the frame to the ambient air. Equation (34) and (35) show the heat transfer between absorber (front) and ambient air as well as the heat transfer coefficient considering the heat conduction through the side insulation and the ratio of the surfaces.

$$\dot{Q}_{a1-edge} = h_{edge} * A_{edge} * (T_{a1} - T_{amb}) \tag{34}$$

$$h_{edge} = \frac{k_c}{d_{edge}} \tag{35}$$

2.7. Overall heat transfer coefficients between the nodes

The thermal resistances R_{th} of the collector connecting the nodes and the ambience are created from a network of the heat transfer coefficients h and the related areas A to calculate a heat flow rate $\dot{Q}$ according to equation (36) [5].

$$\dot{Q}_{1-2} = h_{1-2} * A * (T_1 - T_2) = \frac{1}{R_{th,1-2}} * (T_1 - T_2) \tag{36}$$

Therefore, the electrical analogy is used to generate overall heat transfer coefficients between the nodes by combining single resistances of serial and parallel connections according to Figure 1. The required heat transfer coefficients (related to the area) of the energy fluxes from equations (1) to (5) are shown in the equations (37) to (42).

$$\frac{1}{R_{th,g-amb}} = h_{cond,g} * A + \left(\frac{1}{h_{rad,g-sky} * A} + \frac{1}{h_{conv,g-amb} * A} \right)^{-1} \tag{37}$$

$$\frac{1}{R_{th,a1-g}} = h_{cond,g} * A + \left(\frac{1}{h_{rad,a1-g} * A} + \frac{1}{h_{conv,a1-g} * A} \right)^{-1} + h_{cond,a1} * A \tag{38}$$

$$\frac{1}{R_{th,a1-f}} = h_{cond,a1} * A + h_{conv,a1-f} * A \tag{39}$$

$$\frac{1}{R_{th,f-a2}} = h_{conv,f-a2} * A + h_{cond,a2} * A \tag{40}$$

$$\frac{1}{R_{th,a2-c}} = h_{cond,a2} * A + \left(\frac{1}{h_{rad,a2-c} * A} + \frac{1}{h_{conv,a2-c} * A} \right)^{-1} + h_{cond,c} * A \tag{41}$$

$$\frac{1}{R_{th,c-amb}} = h_{cond,c} * A + \left(\frac{1}{h_{rad,c-amb} * A} + \frac{1}{h_{conv,c-amb} * A} \right)^{-1} \tag{42}$$

2.8. Validation

The model was validated using a parameter set of a tested conventional flat-plate collector. Therefore, the thermal properties of the sheet-pipe absorber had to be additionally implemented in the model.

In a first validation step the developed model was compared to the results of a one-dimensional multi node model approach [2] based on parameters derived from collector testing. The relative deviation of the collector efficiency is in range between -3 % and +1 % for flow temperatures between 25°C and 90°C (Fig. 2).

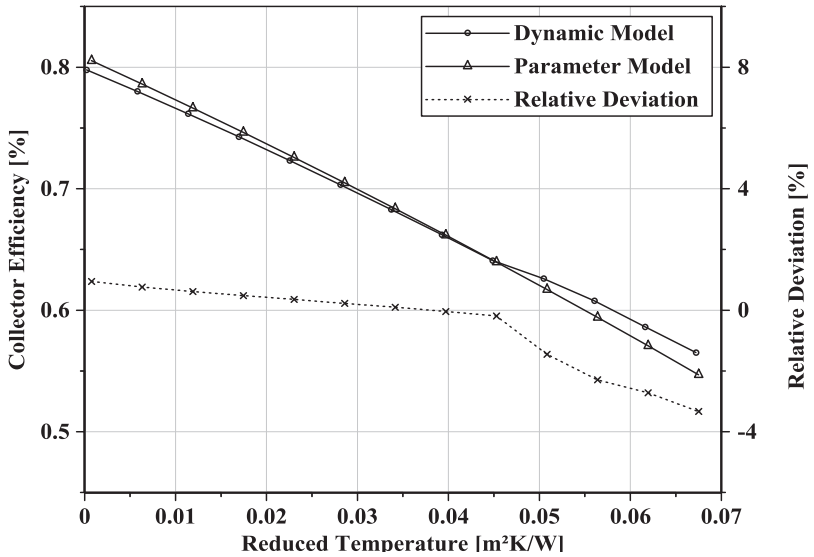

Fig. 2. Comparison of the simulated efficiency curves of the developed dynamic collector model and the parameter model

The deviation is supposed to originate from the rough discretisation in the model like the constant selective behaviour of the coating or the fully developed fluid flow over the riser length without entrance effects. Next to the analysis of efficiency, the models were compared in an annual simulation of a solar-thermal heating system for domestic hot water and space heating. The deviation was found to be 3 %, which is similar to the results of the comparison of efficiency.

In a second step, the simulation results were compared to measurement data from testing and showed satisfying accordance especially with regard to individual part temperatures. During stagnation at insolation of 885 Wm^{-2} and ambient temperature of 33°C, the absorber temperature of model and test differ at +10 K. The average temperatures (3 measurement points) at glazing and backside differ only slightly (Table 1). The reason seems to be model discretisation as well as degradation of the absorber coating, imprecise air gap distances inside the collector, humidity in the mineral wool and dirt on the glazing.

Table 1. Collector part temperatures during stagnation of a conventional flat-plate collector in testing and simulation

	Testing	Model	Difference
Absorber	190°C	200°C	+10 K
Glazing	70°C	70°C	0 K
Backside	55°C	57°C	+2 K

3. Simulation

In order to investigate thermal loads and fractional energy savings of a basic polymeric collector approach in comparison to a conventional collector, a simulation study was performed using the above described model. The model was parameterised with air gaps in the collector of 20 mm, insulation of 20 mm at the backside and 13 mm at the edge (cf. Fig. 1). The optical characteristics of the volumetric polymer absorber were in a first step set to $\alpha = \varepsilon = 0.95$ (non-selective).

As the efficiency curve provides only limited information for the evaluation of the collector designs regarding material choice, an annual system simulation of an exemplary solar-thermal system setup for domestic hot water supply and space heating was conducted. The basic system had a collector area of 16 m² and a buffer store volume of 800 l. The house was simulated for Würzburg (Germany) equipped with oil furnace and floor heating. The heat

energy consumption for floor heating was about 16,500 kWh and 2,500 kWh for domestic hot water. The relevant criterion for evaluation are fractional energy savings f_{sav}, describing the energy fraction being covered by the solar-thermal system in comparison to a heating system without a solar-thermal system. Apart from that, the occurring stagnation temperatures are relevant especially for material selection. However, polymeric materials have temperature durability in the short-term as well as in the long-term sector. Hence, the stagnation temperature gives only an overview on applicable polymeric materials. In the simulation the stagnation test according to EN 12975-2 [14] was carried out meaning that the stagnating dry collector was calculated with insolation of 1,000 Wm^{-2} and ambient temperature of 30°C.

3.1. Conventional flat-plate collectors

As a reference the above described system was simulated with conventional flat-plate collectors. Two scenarios were taken into account - conventional flat-plate collectors with and without selective absorber coating – in order to determine the influence on the system efficiency and the part temperatures.

The system with highly-selective coated absorbers (optical characteristics: $\alpha = 0.95$; $\varepsilon = 0.04$) reaches fractional energy savings (f_{sav}) of 20.0 % and a temperature of 217°C during stagnation. In the same system with a non-selective absorber coating ($\alpha = 0.95$; $\varepsilon = 0.90$), the fractional energy savings decrease to 15.7 % and the maximum temperature reduces to 136°C (cf. Table 2).

Table 2. Fractional energy savings f_{sav} and stagnation temperatures of conventional collectors with and without selective coating

Collector	f_{sav} [%] / efficiency decrease [%]	T_{Stag} [°C]
Reference with selective absorber	20.0 / --	217
Reference without selective absorber	15.7 / -21.5	136

3.2. Polymeric collector approach

The polymeric collector approach was analysed for different scenarios and compared to the conventional collector, shown in Table 3. The stagnation temperature of 128°C for the collector approach without selective coating would in principle be suitable for commodity plastics. However, the decrease of -28.5 % of the fractional energy savings in comparison to the reference system is considerable, which can in this example neither be balanced by an increase of the collector area (-19.0 %) nor by a bigger buffer storage volume (-24.5 %). On the other hand, using the selective coating of the reference collector the system efficiencies as well as the stagnation temperature increase considerably. However, the fractional energy savings are still lower than the reference results. This is caused by the high heat transfer rate via radiation of the absorber backside on the one hand. The copper plate of the absorber of the reference collector has a low emission coefficient ($\varepsilon = 0.019$) in comparison to the emission coefficient of the polymeric absorber ($\varepsilon = 0.95$). On the other hand, the heat transfer through radiation and convection is increased by the reduced insulation of the backside resulting in an increased temperature difference between absorber and inner casing surface.

Table 3. Annual system efficiency and stagnation temperature of polymeric collectors depending on absorber surface, collector area and storage volume

Collector	f_{sav} [%] / efficiency decrease [%]			T_{stag} [°C]
	800 l	800 l	1,200 l	
	16 m²	24 m²	16 m²	
Reference with selective absorber	20.0 / --	--	--	217
Polymeric collector with non-selective absorber	14.3 / -28.5	16.2 / -19.0	15.1 / -24.5	128
Polymeric collector with selective absorber	18.3 / -8.5	20.5 / +2.5	19.7 / -1.5	184

In the system simulations the absorber temperature of the non-selective reference collector reaches 139°C whereas the non-selective polymeric collector approach has a temperature of maximum 126°C. Also the durations at temperatures above 75°C are substantially longer (cf. Figure 3).The selective absorber in the reference collector reaches 223°C and the selective polymeric collector with reduced efficiency has 189°C and a significant reduction of the temperature loads above 165°C.

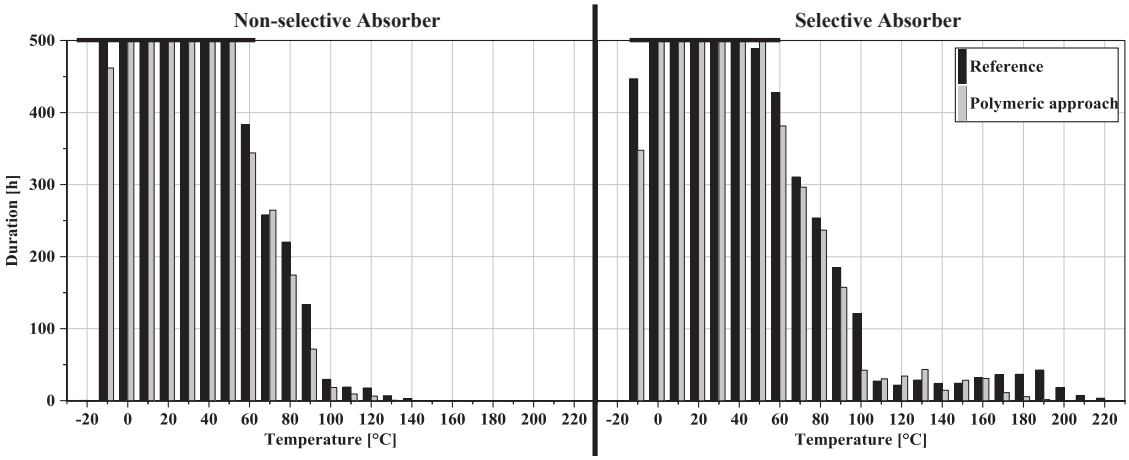

Fig. 3. Histograms of the absorber temperature of the collector models in the standard system over one year

The polymeric insulation of the collector approaches has its highest temperatures behind the absorber inside the collector (Figure 4). The non-selective collector has a maximum temperature of 111°C and quite low durations at temperature levels above 85°C. The maximum temperature of the polymeric collector with selective absorber is 151°C. The durations at high temperatures are quite long in regions above 100°C. Therefore, a temperature resistant material of commodity plastics would be required.

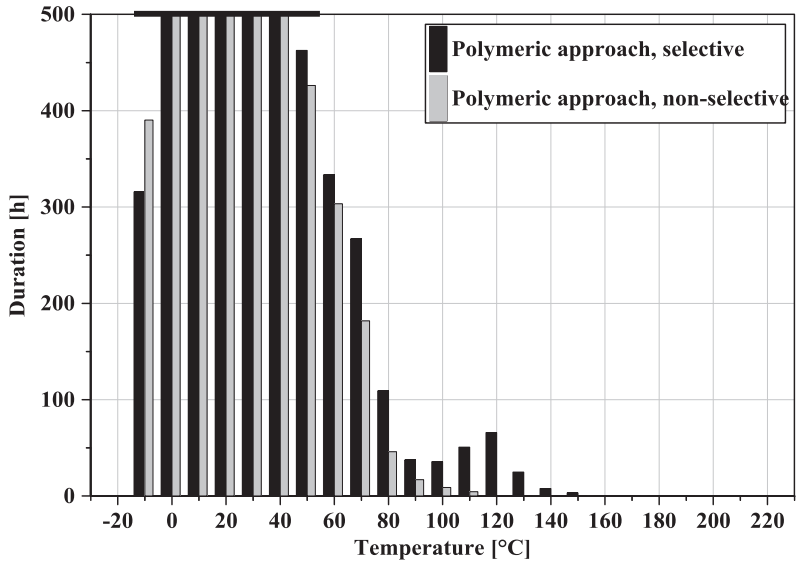

Fig. 4. Histogram of the inner insulation temperature of the polymeric collector models in the standard system over one year

4. Conclusions

A detailed dynamic model for the analysis of polymeric collector designs was developed. Validation using experimental results of conventional flat-plate collectors showed satisfying results especially regarding the calculation of individual part temperatures of a collector. The simulation results showed that the fractional energy savings of systems with conventional flat-plate collectors cannot be reached with the analysed polymeric collector approach. Also the stagnation temperatures of more efficient approaches are too high for low-cost polymeric materials. The exemplary analysis of annual temperature loads of the backside insulation for different approaches proved the necessity of careful collector design aiming at temperature reduction for all individual collector parts.

References

[1] MathWorks, Inc. Simulink. http://www.mathworks.com/help/toolbox/simulink/index.html [Accessed: 20/09/13].
[2] Hafner B, Plettner J, Wemhöner C. Carnot Blockset Version 1.0 - Conventional and renewable energy systems optimization blockset - User's guide. Solar-Institut Jülich, Fachhochschule Aachen; 1999.
[3] Duffie J, Beckman WA. Solar Engineering of Thermal Processes. 2nd ed. New York: Wiley; 1991.
[4] Eicker U. Solar Technologies for Buildings. 1st ed. Chichester: Wiley; 2003.
[5] Stephan P. VDI Heat Atlas. 2nd ed. Düsseldorf: VDI-Verlag GmbH; 2010.
[6] Mills AF, Heat Transfer. 2nd ed. New Jersey: Prentice Hall; 1999.
[7] Gnielinski V. Ein neues Berechnungsverfahren für die Wärmeübertragung im Übergangsbereich zwischen laminarer und turbulenter Rohrströmung. Forschung im Ingenieurwesen 61:240-248; 1995.
[8] Gnielinski V. New equations for heat and mass transfer in turbulent pipe and channel flow. International Journal of Chemical Engineering 16:359-369; 1974.
[9] Schlichting H Grenzschicht-Theorie. 3rd edn. Verlag G. Braun, Karlsruhe; 1958.
[10] Fujii T, Imura H. Natural-convection heat transfer from a plate with arbitrary inclination. International Journal of Heat and Mass Transfer 15:755-767; 1972.
[11] Matuska T, Zmrhal V. KOLEKTOR 2.2 – reference handbook. 1st ed. Prague: Czech Technical University.
[12] Hollands et al. Free convective heat transfer across inclined air layers. Journal of Heat Transfer 98:189-193; 1976.
[13] Arnold et al. Experimental investigation of natural convection in inclined rectangular regions of differing aspect ratios. ASME parer 75-HT-62; 1975.
[14] EN 12975-2. Thermal solar systems and components – Solar collectors – Test methods. European Committee for Standardisation. Brussels; 2001.